Thermodynamic phase diagram, phase competition, and uniaxial pressure effects in $BaFe_2(As_{1-x}P_x)_2$ studied by thermal expansion

A. E. Böhmer,[1,2] P. Burger,[1,2] F. Hardy,[1] T. Wolf,[1] P. Schweiss,[1] R. Fromknecht,[1] H. v. Löhneysen,[1,3] C. Meingast,[1] H. K. Mak,[4] R. Lortz,[4] S. Kasahara,[5] T. Terashima,[5] T. Shibauchi,[6] and Y. Matsuda[6]

[1]*Institut für Festkörperphysik, Karlsruhe Institute of Technology, 76021 Karlsruhe, Germany*
[2]*Fakultät für Physik, Karlsruhe Institute of Technology, 76128 Karlsruhe, Germany*
[3]*Physikalisches Institut, Karlsruhe Institute of Technology, 76128 Karlsruhe, Germany*
[4]*The Hong Kong University of Science & Technology, Clear Water Bay, Kowloon, Hong Kong*
[5]*Research Center for Low Temperature and Materials Sciences, Kyoto University, Kyoto 606-8501, Japan*
[6]*Department of Physics, Kyoto University, Kyoto 606-8502, Japan*

(Received 12 March 2012; revised manuscript received 5 September 2012; published 24 September 2012)

High-resolution thermal-expansion and specific-heat data of isovalently substituted single-crystalline $BaFe_2(As_{1-x}P_x)_2$ ($0 \leqslant x \leqslant 0.33$, $x = 1$) are presented. We show that crystals can be detwinned *in situ* in the capacitance dilatometer, allowing a study of all three independent crystallographic directions. From the thermal-expansion data, we determine the phase diagram via a thermodynamic probe, study the coupling of the spin-density wave (SDW) and superconducting order parameters, and determine various pressure dependencies of the normal and superconducting states. Our results show that in the underdoped region, superconductivity and SDW order coexist and compete with each other. The resulting phase diagram, however, exhibits a smaller coexistence region of SDW and superconductivity with a steeper rise of T_c on the underdoped side than in, e.g., $Ba(Fe_{1-x}Co_x)_2As_2$. On the overdoped side, where there is no sign of SDW order, the lattice parameters respond to superconductivity in much the same way as to the SDW on the underdoped side, which demonstrates the intimate connection between both kinds of order. Using thermodynamic relations, the uniaxial pressure derivatives of the superconducting critical temperature and the electronic Sommerfeld coefficient are determined from our thermal-expansion data together with the specific-heat data. We find that uniaxial pressure is proportional to P substitution and that the electronic density of states has a maximum at optimal doping. Overall, the coupling of the SDW and superconducting order to the lattice parameters of $BaFe_2(As_{1-x}P_x)_2$ is found to be qualitatively very similar to that of the well-studied, supposedly electron-doped $Ba(Fe_{1-x}Co_x)_2As_2$ system.

DOI: 10.1103/PhysRevB.86.094521 PACS number(s): 74.70.Xa, 74.25.Bt, 74.62.Dh, 74.62.Fj

I. INTRODUCTION

In the intensively studied 122 family of iron-based superconductors, superconductivity can be induced by various substitutions in $BaFe_2As_2$ (Ba122), e.g., K for Ba, Co or Ru for Fe, and also P for As, as well as by hydrostatic pressure.[1–6] In all cases, the resulting phase diagrams are surprisingly similar: a superconducting dome arises around the doping level or pressure where the magnetostructural transition of the parent compound is suppressed to zero temperature. This raises the question of the detailed physical mechanism leading from the spin-density wave (SDW) to superconductivity using these different tuning parameters. The isovalent substitution of As by P in $BaFe_2(As_{1-x}P_x)_2$ (P-Ba122) with a maximum T_c of 30 K is particularly interesting since (nominally) no additional charge carriers are introduced. Here, it has been suggested that superconductivity is induced by a chemical pressure effect.[4,5,7] It was also found that the phase diagram of P-Ba122 can be tracked from any starting P concentration[7] using hydrostatic pressure, suggesting that pressure is somehow equivalent to additional doping, as has also been found for the Co-doped system.[8,9] In contrast to Co doping, P substitutions do not appear to introduce significant disorder as evidenced by the observation of de Haas–van Alphen (dHvA) signals for $0.41 < x < 1$ (Refs. 10 and 11) and the absence of quasiparticle scattering in vortex pinning.[12] The low scattering rate for P substitutions is one reason why this may be an ideal system for further study. Evidence for a quantum critical point close to optimal doping was obtained from non-Fermi-liquid transport,[5] nearly zero Curie-Weiss temperature in NMR,[13] and mass enhancement in dHvA measurements.[10]

Recent studies on Co-Ba122 showed that both magnetic and structural order parameters are reduced in the superconducting state.[14–16] This has been interpreted as evidence for microscopic coexistence and competition between the orthorhombic SDW phase and superconductivity in the underdoped region of the phase diagram.[14,17] In some of the 1111 compounds, on the other hand, no such coexistence region has been observed,[18] and it is still debated whether magnetism and superconductivity coexist microscopically in K-doped Ba122.[19–21] It is thus of great interest to study the interplay of magnetism and superconductivity also in P-Ba122.

In this paper, the thermodynamic phase diagram, the interplay of structural/magnetic order and superconductivity, as well as the effects of uniaxial pressure on normal and superconducting state properties of $BaFe_2(As_{1-x}P_x)_2$ are investigated by thermal-expansion measurements, complemented with specific-heat and magnetization data. Throughout the paper, we will compare our results to those of the Co-doped system, for which several detailed thermal-expansion studies already exist.[9,22,23] One main result of our study is that both P- and Co-substituted systems behave qualitatively very similar. In particular, not only the phase diagrams, but also the uniaxial pressure derivatives of the transition temperatures, as well as the coupling of the order parameters, turn out to be quite

similar in both systems. Both kinds of substitutions can also be directly linked to uniaxial pressure, and both systems display a maximum of the Sommerfeld coefficient at optimal doping. The interesting question of why these systems behave so similar, in spite of the presumably different routes (chemical pressure versus electron doping) to superconductivity, will be addressed at the end of the paper. Please note that throughout the paper the term "doping" will be used in a broad sense, as an equivalent to substitution.

The paper is organized as follows. In Secs. II and III, we present the experimental details and results, from which we construct the thermodynamic phase diagram (Sec. IV). In Sec. V, we discuss the interplay of the structural/magnetic order with superconductivity. The uniaxial pressure effects on T_c and the electronic density of states are presented in Sec. VI, and conclusions are provided in Sec. VII. A brief preliminary report[24] on parts of this work has been presented previously.

II. EXPERIMENTAL DETAILS

Single crystals of P-substituted Ba122 were grown from stoichiometric mixtures of the starting materials as described in Ref. 5. Crystals of pure $BaFe_2P_2$ were grown from self-flux using an Al_2O_3 crucible in a closed steel container. Ba and prereacted FeP were mixed in a ratio of 1:5, heated up to 1300 °C and slowly cooled down to 1200 °C at a rate of 0.3 °C/h. The typical crystal size is $\sim 500 \times 500 \times 100\,\mu m^3$. Four-circle x-ray structural refinements were conducted on three of our samples and yielded a P content of $x = 0.25(1), 0.30(1), 0.33(1)$. The P content of the other samples [$x = 0.12(2), 0.18(2), 0.26(2), 0.27(2)$] was determined by energy-dispersive x-ray analysis (EDX) on these samples and complemented by four-circle x-ray diffraction on samples from the same batch, hence the larger error.

Thermal expansion was measured in a home-built capacitive dilatometer with a typical resolution of 0.1–0.01 Å (Ref. 25). In the dilatometer, the sample is pressed against one plate of a plate-type capacitor (with a force of $F \approx 0.2$ N) so that a change of the sample length results in a changing capacitor gap. Samples were mechanically detwinned *in situ* by mounting them such that the dilatometer pressure is directed along their tetragonal [110] direction.[26] In this configuration, thermal expansion along the (shorter) orthorhombic b axis is measured. Comparison with twinned samples, for which the dilatometer pressure is applied along the tetragonal [100] direction, allows us to estimate the thermal expansion along the orthorhombic a axis as well. Accurate data could be obtained in spite of the (for dilatometry) extremely small sample size.

The specific heat on the tiny samples with masses in the order of 100 micrograms was measured with a home-made microrelaxation calorimeter using a "long-relaxation" technique.[27] Each relaxation at different base temperature provides about 1000 data points over a temperature interval of up to 50% above the base temperature. Magnetization was measured with a commercial Quantum Design vibrating-sample superconducting quantum interference device (VSM-SQUID).

III. RESULTS

Figure 1 shows the measured uniaxial thermal-expansion coefficients $\alpha_i = (1/L_i) dL_i/dT$ where L is the sample length and the subscript i stands for the direction. Clear anomalies are observed at the magnetostructural transition (at T_{sm}) and at the onset of superconductivity at T_c^{on} as indicated in the figure. Panel (b) shows the detwinned measurements of underdoped samples, which become orthorhombic upon cooling. It is clear that the process of detwinning strongly enhances all anomalies when compared to the twinned measurements [panel (a)]. In order to look for a possible splitting at the magnetostructural transition into two transitions, we present a detailed comparison of twinned, detwinned, and c-axis data in panels (e) and (f) of Fig. 1 for $x = 0.18$ and 0.25, respectively. Only a single peak at T_{sm} is discernible in the c-axis data for the $x = 0.25$ sample, whereas there appears to be an additional shoulder a few degrees above the peak at T_{sm} for the $x = 0.18$ sample. The twinned data give very similar transition temperatures as the c-axis data and also do not show clear evidence for a split transition. From these data, we estimate that a possible splitting of the magnetostructural transition amounts at most to ∼2–4 K. The peaks in the detwinned data, in which uniaxial pressure is applied along the tetragonal [110] direction, show a significant broadening and a slight upward shift (∼3 K) in temperature, in line with theoretical expectations.[28] Since we are unable to determine split transition temperatures reliably, we choose to refer to a joint magnetostructural transition, bearing in mind that a small splitting can not be ruled out.

Samples with $x \geqslant 0.25$ show bulk superconductivity. The onset of superconductivity on the underdoped side is signaled by a rather sharp kink (at T_c^{on}) followed by a broad peak, which has the opposite sign of the anomaly at the structural transition. We use an area-conserving construction [see Fig. 2 (e)] to define a T_c^{mid}. On the overdoped side ($x = 0.33$), the anomaly at T_c has the usual, steplike shape expected at a second-order phase transiton, and T_c^{on} and T_c^{mid} nearly coincide. Note that the sign of the thermal-expansion anomaly allows us to assign a sample uniquely to lying either on the underdoped or on the overdoped side. The anomalies of the thermal-expansion coefficient along the c axis [Fig. 1 (c)] have similar shape but opposite sign as compared to the in-plane measurements in all cases. It is important to note that the anomalies of the α_i's have the same sign and exhibit a very similar shape as reported for the $Ba(Fe_{1-x}Co_x)_2As_2$ (Co-Ba122) system.[9,22,23] Since $\alpha_i \propto -dS/dp_i$ (uniaxial pressure derivatives of the entropy), this shows that the entropy of the two systems responds similarly to uniaxial pressure. This will be discussed in more detail in Sec. VI.

The strikingly different shape of the superconducting transition of underdoped and overdoped samples is also seen in other measurements. Figure 2 shows the superconducting transition of the underdoped ($x = 0.27$) and overdoped ($x = 0.33$) P-Ba122 samples in the dc magnetization, the electronic specific heat (derived by subtracting the lattice heat capacity of an undoped Ba122 sample), and the thermal expansion. For underdoped $BaFe_2(As_{0.73}P_{0.27})_2$, there is a sharp onset at T_c^{on} in all three data sets, however, the main anomaly appears very broad and rounded. The approximate transition width is

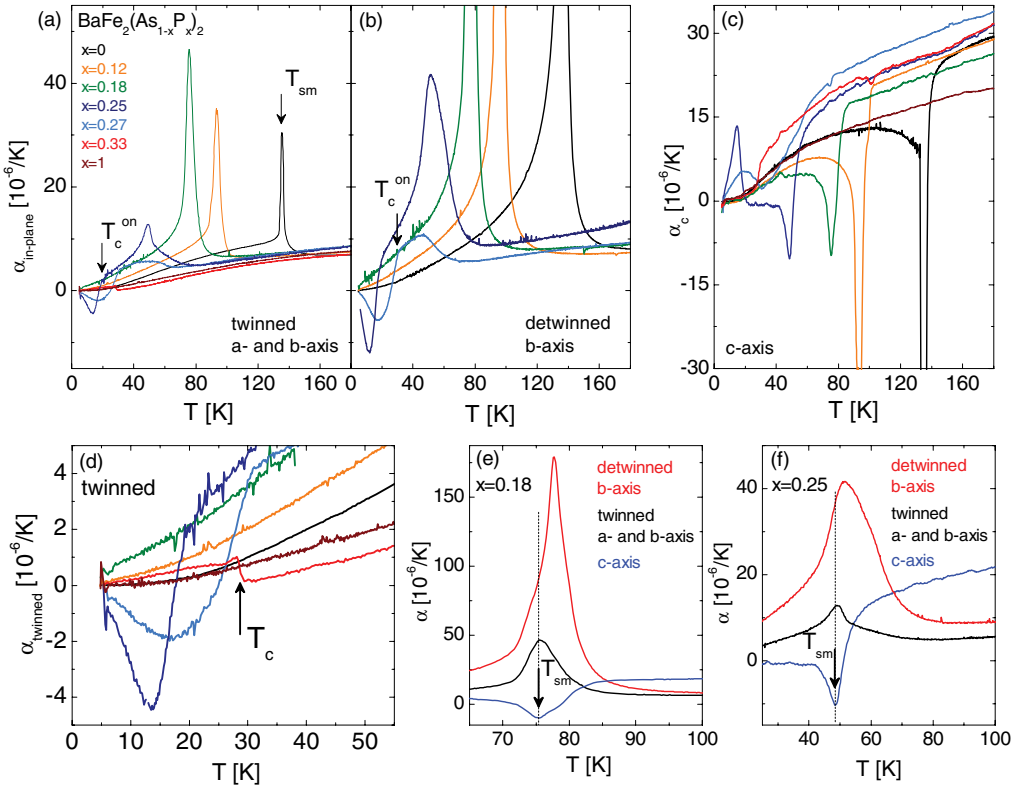

FIG. 1. (Color online) Uniaxial thermal-expansion coefficients α_i as a function of temperature T for (a) twinned in-plane and (b) detwinned measurements (along the b axis) and (c) along the c axis for various substitution levels as indicated in panel (a). Arrows indicate examples of the temperature of the magnetostructural transition $T_{\rm sm}$ and $T_c^{\rm on}$. (d) Magnified view of the low-temperature region of (a). (e) and (f) show a comparison of twinned, detwinned, and c-axis data around the magnetostructural transition temperature for $x = 0.18$ and 0.25, respectively.

10–15 K. On the other hand, overdoped $BaFe_2(As_{0.67}P_{0.33})_2$ exhibits sharp, steplike anomalies of α, C_p, and M at T_c. A possible origin of the broadening in the underdoped samples will be presented in Sec. IV.

IV. PHASE DIAGRAM

Figure 3 shows the phase diagram compiled from the present thermodynamic data together with previous work on resistivity[5] of the same system and thermodynamic data for Co-Ba122 (Refs. 9 and 29), which have been scaled so that the optimal doping concentrations of both systems coincide. $T_{\rm sm}$ in the P-substituted system has been determined uniquely from the c-axis measurements, which we judge to give the most reliable results because of two reasons. First, the applied pressure during c-axis measurements is 5–10 times smaller than for in-plane measurements due to the platelike shape of the crystals. Second, since c-axis pressure does not directly couple to the orthorhombic order parameter, the transition should remain sharp and not turn into a crossover, as for in-plane pressure.[28,30,31]

In underdoped P-Ba122, the bulk T_c obtained from thermal expansion is lower than T_c inferred from resistivity. Furthermore, the thermodynamic measurements reveal a very steep slope of T_c. This may offer a simple explanation for the broad superconducting transitions of the underdoped samples of P-Ba122 (Fig. 2). For a given concentration gradient in the sample, the width of the transition will be directly related to this slope. For $x = 0.25$–0.27, the width of T_c amounts to 10–15 K, while it is only $\sim$1 K on the overdoped side. This difference can thus be explained by the roughly 13 times greater slope of T_c on the underdoped side. However, the sharp kinks at $T_c^{\rm on}$ remain unexplained. We note that quite broad superconducting transitions on the underdoped side have also been reported previously from resistivity[5] and susceptibility[32] measurements.

We have already noted that the response of the entropy to uniaxial pressure is very similar for P-Ba122 and Co-Ba122. Overall, their phase diagrams are also very similar, however, they also show some differences. First, on the underdoped side, the bulk T_c rises more steeply in P-Ba122 than in the Co-doped system. This may be a signature of a stronger competition between the SDW and the superconducting phase. A steep rise of the transition line signals that two phases differ little in entropy so that only a significant increase of temperature triggers the transition. This means that here, superconductivity is not much "weaker" than magnetism, and a strong influence of the two types of order on each other is expected.

A second difference of the phase diagrams of P-Ba122 and Co-Ba122 is that the splitting of the magnetostructural transition is much smaller or even nonexistent in the P-substituted system. The reduced magnitude of the splitting may be explained by less scattering in the P-substituted samples.[12] A reduction of the splitting with decreasing disorder has been reported previously in the 1111 systems.[33] Finally, on the overdoped side, T_c is uniformly higher for P substitution than for Co substitution, possibly also due to less disorder.

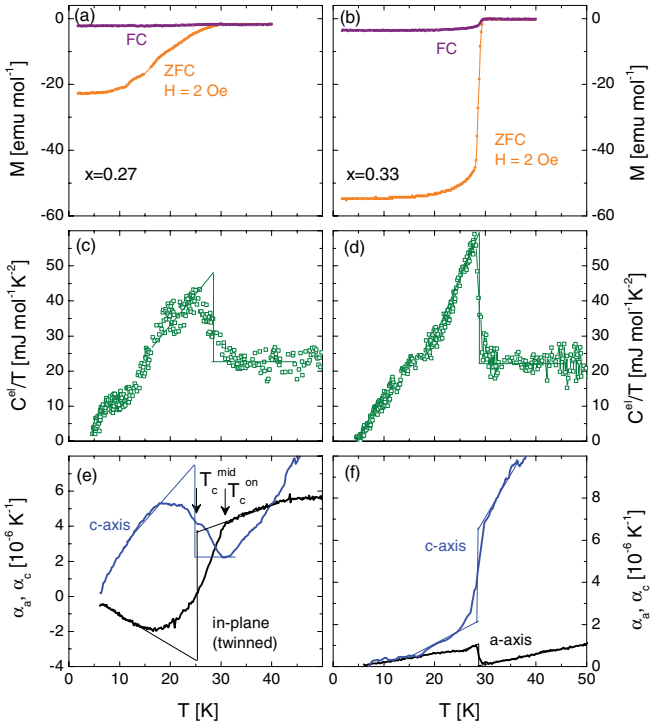

FIG. 2. (Color online) The superconducting transition of samples with $x = 0.27$ (underdoped, left column) and $x = 0.33$ (overdoped, right column) seen by different probes. Magnetization [panels (a) and (b)], specific heat [panels (c) and (d)], and thermal expansion [panels (e) and (f)] all show a broad superconducting transition with a sharp onset for the underdoped sample and more standard, sharp anomalies for the overdoped sample. The lines in panels (c)–(f) represent idealized second-order transitions.

V. INTERPLAY OF ORTHORHOMBICITY, SDW, AND SUPERCONDUCTIVITY

In the following, we will use our thermal-expansion data to study the interplay between structural/magnetic and superconducting order parameters. As an example, Fig. 4 shows the relative length changes of the $x = 0.25$ sample. We note that only the b and the c axes can be measured directly. The a axis is derived from the difference between in-plane twinned and detwinned data, and the orthorhombic order parameter $\delta = (a - b)/(a + b)$ (inset of Fig. 4) is derived from the difference between the a and b axes.

The a and b axis lengths start to differ clearly at the structural transition, and this difference is directly proportional to the structural order parameter in this system. There exists a high-temperature tail to the transition, which arises from the small applied in-plane pressure of the order of 5–10 MPa.[30,31] Clearly, a and b axes approach each other again below T_c and the orthorhombic order parameter decreases, suggesting a similar coupling of structural and superconducting order parameters as observed in Co-Ba122 (Ref. 16). Interestingly, the c-axis length increases below T_{sm} and then decreases below T_c, and thus exhibits a very similar behavior as the in-plane axes. We note that the effect of these transitions on the volume is very small (see Fig. 4) due to an almost complete cancellation of the anomalies along the different directions.

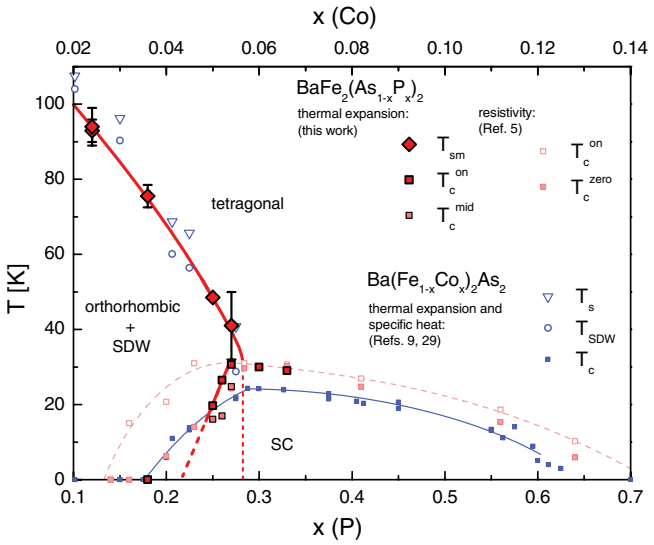

FIG. 3. (Color online) Thermodynamic phase diagrams of P-Ba122 (lower axis) compiled from the present thermal-expansion data and of Co-Ba122 (upper axis) scaled so that the maximum T_c's coincide. Data for Co-Ba122 were obtained from specific-heat (Ref. 29) and thermal-expansion (Ref. 9) measurements. Also added are previously published resistivity data (Ref. 5) on the P-Ba122 system (onset of superconducting transition T_c^{on} and temperature where zero resistivity is achieved T_c^{zero}).

In Figs. 5 and 6, we show the temperature-dependent length changes of the b and c axes, respectively, for different doping levels. Please note that we do not show the calculated a-axis data, and thus the orthorhombic order parameter, for all doping levels because partial detwinning occurred during some of the twinned measurements, which results in some uncertainty in this procedure. However, the temperature dependence of δ is also reflected in the (negative) b-axis length since the a and b axes are found to evolve nearly symmetrically.

The parameter Δb_{tot}, defined to quantify the total change of the b-axis length due to the magnetostructural transition, is shown in the inset of Fig. 5. Δb_{tot} decreases linearly with P content confirming reliable detwinning. Exceptions are the samples with $x = 0.26$ and 0.27. Even though the transition temperatures are similar, Δb_{tot} is much smaller for these samples and does not follow T_s any more. Possibly, only a part of the sample undergoes the magnetostructural transition. Similarly, NMR found evidence that a fraction of a collection of samples with $x = 0.25$ does not undergo the SDW transition.[32] Hence, we exclude the samples with $x = 0.26$ and 0.27 in the analysis of the electronic part of the thermal expansion (Sec. VI).

The "electronic c-axis length changes" ΔL_c^{el} shown in Fig. 6(b) are obtained by subtracting the $x = 1$ data as lattice background using a correction factor to account for the uncertainties in the measurements.[34] We use the $x = 1$ data as a lattice background because pure $BaFe_2P_2$ does not undergo any phase transitions and, additionally, the electronic contribution to its thermal expansion is negligibly small compared to the effects discussed here.

The coupling between SDW order and superconductivity can be directly observed in both b-axis and c-axis data shown in

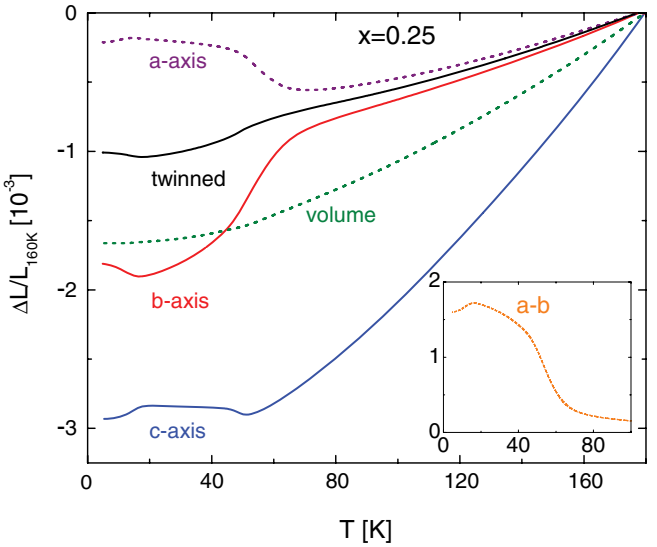

FIG. 4. (Color online) Relative change of sample length of the $BaFe_2(As_{0.75}P_{0.25})_2$ sample, measured in the twinned (in-plane average, black line) and detwinned (b axis, red line) configuration and along the c axis (blue line). The a-axis length (broken purple line) was estimated from the twinned and detwinned in-plane measurements and the volume change (green broken line) from the twinned in-plane and the c-axis measurements. The inset shows the difference of a axis and b axis. For this sample, $T_{sm} = 48.5$ K and $T_c^{mid} = 16$ K.

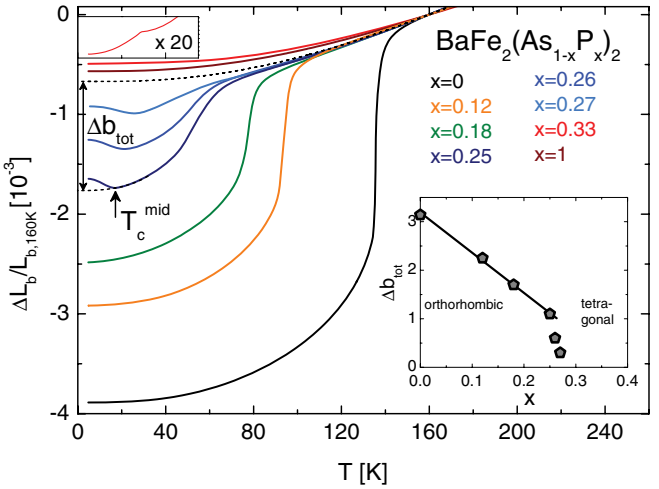

FIG. 5. (Color online) Relative change of the b-axis length (in-plane length for the overdoped samples) for various doping levels. Its shortening signals the magnetostructural transition, and its increase below T_c for the superconducting samples demonstrates the competition between the orthorhombic phase and superconductivity. The upper inset shows the data for $x = 0.33$ on an expanded vertical scale. The lower inset shows the doping evolution of Δb_{tot} as defined in the main panel. The reference lines for the determination of Δb_{tot} (dashed black lines) are a smooth extrapolation. The upper line is provided by the data for $x = 1$ scaled with a constant factor.

Figs. 5 and 6. For both axes, the effect of superconductivity is to reduce the SDW induced distortions in the lattice parameters, strongly suggesting that both phases coexist and compete with each other. This is very similar to the direct coupling of the structural orthorhombic and superconducting order parameters observed previously in Co-doped Ba122 (Ref. 16). Especially of interest in our data is that the behavior of ΔL_c^{el} also closely resembles the behavior of the the orthorhombic order parameter. Although it is not clear how, or if at all, the c-axis response can be directly linked to the structural/magnetic order parameters, our results show that the SDW state favors a longer c axis. Equivalently, compressing the c axis by uniaxial pressure will destabilize magnetism. This is in agreement with density functional theory (DFT) calculations under uniaxial pressure.[35] The decrease of the c-axis length upon entering the superconducting state is thus consistent with a suppression of magnetism by superconductivity.

Intriguingly, the lattice parameters of the overdoped $x = 0.33$ sample respond in an opposite way to the onset of superconductivity as compared to the underdoped samples. We find that the superconducting state in the absence of static magnetic order in fact favors a longer c axis in a similar manner as does the SDW state of underdoped P-Ba122. The same effect, although much smaller in magnitude, is also seen for the in-plane dimension: The in-plane length of overdoped P-Ba122 decreases (slightly) in response to superconductivity, as does the average in-plane length of the underdoped material upon entering the SDW state. The similar response of the lattice parameters to SDW and superconductivity in the absence of SDW order actually may hint at a kinship of both ordering phenomena, despite their competitive relationship in the coexistence region. In Co-Ba122, this is also suggested by nearly identical Grüneisen-parameters of the two phases.[9]

Finally, we address the question of microscopic coexistence of magnetism and superconductivity. Dilatometry is a macroscopic probe, and the T dependence of a sample length can not *a priori* be equated with the T dependence of the lattice parameters if one has a phase-separated sample. Still, the close resemblance between our results and the evolution of lattice parameters of Co-Ba122 observed by x-ray diffraction[16] is most naturally explained by homogeneous coexistence and competition of magnetism and superconductivity also in P-Ba122. This is in agreement with recent NMR study[32] on P-Ba122, which also concluded that SDW and superconductivity coexist microscopically but compete with each other.

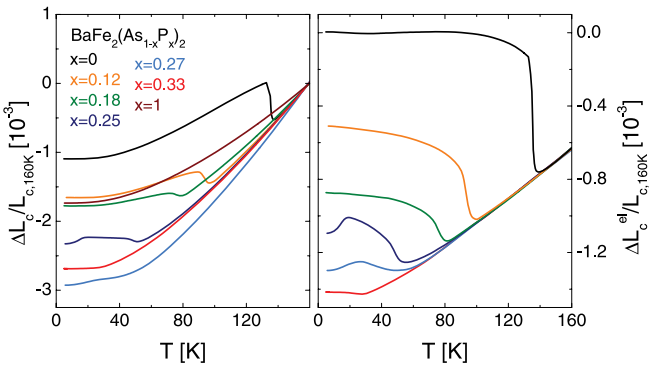

FIG. 6. (Color online) (a) Relative change of the c-axis length for various doping levels. Panel (b) shows the data after subtraction of a background (the data for $x = 1$ times an individual factor close to 1, see text and Ref. 34).

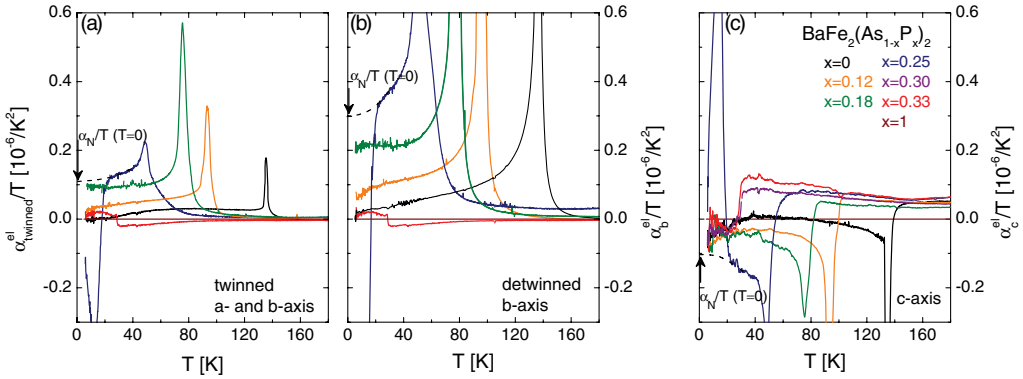

FIG. 7. (Color online) The electronic contribution to the uniaxial thermal-expansion coefficients divided by T, $\alpha_{\rm el}/T$, obtained from subtracting the data of the $x = 1$ sample as a phonon background (a) in the twinned in-plane measurements, (b) along the orthorhombic b axis (detwinned in-plane measurements), and (c) along the c axis. Arrows and dashed lines indicate how values of the normal state $\alpha_i^{\rm el}/T(T = 0)$, which are reported in Fig. 8, are extracted.

VI. UNIAXIAL PRESSURE EFFECTS

For second-order phase transitions, uniaxial pressure derivatives of the transition temperature dT_c/dp_i can be deduced from the jumps of the thermal-expansion coefficient $\Delta\alpha_i$ and the specific heat ΔC_p. For the overdoped, tetragonal sample ($x = 0.33$, $T_c = 29$ K), clear second-order jumps in the uniaxial thermal-expansion coefficients $\Delta\alpha_a = 0.9(2) \times 10^{-6}$ K^{-1}, $\Delta\alpha_c = -4.0(5) \times 10^{-6}$ K^{-1}, and the specific heat $\Delta C_p/T_c = 38(4)$ mJ mol^{-1} K^{-2} are observed (see Fig. 2). The magnitude of the specific-heat jump is in good agreement with data of a recent report by Chaparro *et al.*[36] dT_c/dp_i can be calculated via the Ehrenfest relation

$$\frac{dT_c}{dp_i} = V_m \frac{\Delta\alpha_i}{\Delta C_p/T_c}, \qquad (1)$$

where $V_m = 59.6$ cm^3/mol (Ref. 5) is the molar volume. The data yield $dT_c/dp_a = 1.4(5)$ K/GPa and $dT_c/dp_c = -6.3(1.2)$ K/GPa. The hydrostatic pressure derivative $dT_c/dp = 2dT_c/dp_a + dT_c/dp_c = -3.5(2.2)$ K/GPa is in reasonable agreement with high-pressure experiments[37] which report an initial slope of $dT_c/dp = -1.8$ K/GPa for a sample with $T_c = 30.5$ K. The same kind of anisotropy and a similar magnitude of the uniaxial pressure derivatives have been observed for a slightly overdoped Co-Ba122 crystal.[22] The pressure derivatives on the underdoped side are more difficult to extract due to the large widths of the transitions. However, it is clear that the dT_c/dp_i's are of opposite sign and by far larger in magnitude than those of the overdoped sample. Using the construction for the jumps shown in Fig. 2(e), we find for the $x = 0.27$ sample $dT_c/dp_{ab} = -18(8)$ K/GPa, $dT_c/dp_b = -44(17)$ K/GPa, and $dT_c/dp_c = 20(8)$ K/GPa. Here, p_{ab} refers to an average of pressure along the a and b axes, as is relevant to the twinned in-plane measurements.

Since ΔC_p is always positive, the sign of the anomalies in the α_i provide information on the anisotropy of the dT_c/dp_i even in the absence of specific-heat data. Strikingly, the uniaxial pressure derivatives of $T_{\rm sm}$ have the opposite sign to the derivatives of T_c for all directions.[24] This is again consistent with a competition between the orthorhombic SDW phase and superconductivity since pressure will favor either the SDW or superconducting phase at the expense of the other. Interestingly, all signs of the derivatives can be accounted for by identifying uniaxial pressure with a shift in the P content: stress along the c axis (and a axis on the underdoped side) corresponds to an increased P content, while stress along the b axis (averaged in-plane axis) corresponds to a lower P content. This means that the phase diagram may be tracked (forwards or backwards) by the application of uniaxial pressure just as it can be tracked by hydrostatic pressure.[7] By comparing the values of dT_c/dp_i obtained above with the respective slopes in the phase diagram $dT_c/dx = 6.7$ K/at.%(P) (underdoped) and $dT_c/dx = -0.5$ K/at.%(P) (overdoped), one can estimate that increasing the P content by 1 at.% corresponds to a uniaxial pressure of -0.35 GPa (-0.15 GPa) in the in-plane average (along the b axis). The lower accuracy of the c-axis data unfortunately does not allow such a quantitative analysis.

Thermal-expansion data can also be used to obtain information about the (uniaxial) pressure dependence of the electronic density of states. For a Fermi liquid, the electronic thermal expansion divided by T, $\alpha_i^{\rm el}/T$, is expected to be a constant $\alpha_{{\rm el},i}/T = -(1/V_m)d\gamma/dp_i$, with γ the Sommerfeld coefficient. [This follows directly from $\alpha_i = -(1/V_m)dS/dp_i$ and the electronic specific heat $C = \gamma T$.] Figure 7 shows the electronic/magnetic thermal-expansion coefficients $\alpha_i^{\rm el}/T \propto -d\gamma/dp_i$, which were obtained from the original data by subtracting the data for $x = 1$ as a phonon background using no correction factor (see Sec. V). With increasing doping, a sizable contribution from electronic/magnetic degrees of freedom evolves below the SDW transition for all three crystal directions. Especially for the $x = 0.18$ data, this contribution is nearly independent of temperature up to about 60 K, consistent with Fermi-liquid-type behavior. This is reminiscent of what is observed in weak itinerant ferromagnetic systems, such as MnSi (Ref. 39), and points to an intricate mixing of highly pressure-dependent electronic and magnetic degrees of freedom. For $x = 0.25$, $T_{\rm sm}$ and T_c are too close to each other so that this constant term in $\alpha_{\rm el}/T$ is not seen.

Panel (a) of Fig. 8 shows $\alpha_i^{\rm el}/T(T = 0)$, obtained by extrapolating the normal state $\alpha_i^{\rm el}/T$ data to zero, and corresponding $d\gamma/dp_i$ values versus P substitution. There is a

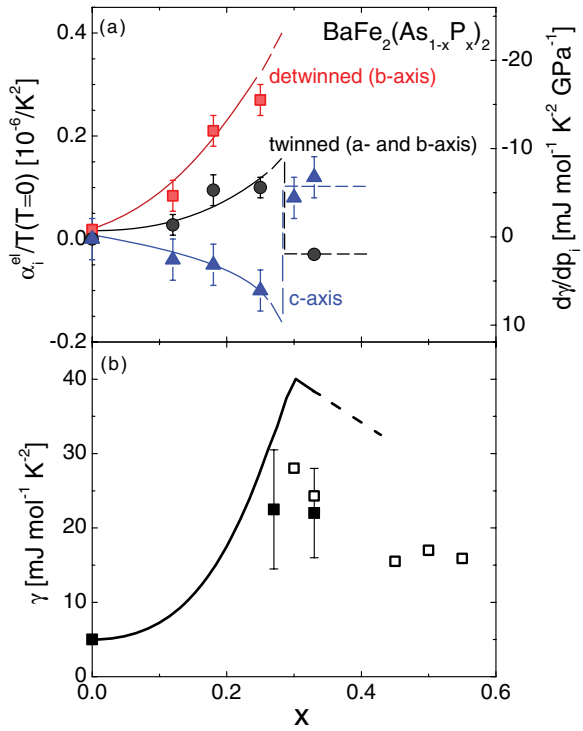

FIG. 8. (Color online) (a) Values of the electronic thermal expansivity $\alpha_{\mathrm{el},i}/T$ extrapolated to zero temperature. The right-hand scale shows the corresponding values of $d\gamma/dp_i$. Lines are a guide to the eye. (b) The Sommerfeld coefficient γ obtained by integrating the smooth lines from (a) (black line) (see text for details). Full squares indicate directly measured values of γ and open squares indicate values estimated from the measured specific-heat jump (Ref. 36) (see also Ref. 38).

sharp increase in the magnitude of $d\gamma/dp_i$ upon approaching optimal doping and a sign change when passing to the overdoped side. The discontinuity of the derivatives $d\gamma/dp_i$ at optimal doping is also suggested from an analogy with the Co-doped system.[9,29] We can obtain γ as a function of x from integration of these data if, as before, we equate doping with pressure. We recall that we can link average in-plane (c-axis) pressure to a decreased (increased) P content. As is evident from the sign change then, $\gamma(x)$ has a maximum at optimal doping. More quantitatively, the proportionality factors from above [$dp_{ab}/dx = -0.35$ GPa/at.%(P) and $dp_b/dx = -0.15$ GPa/at.%(P)] yield values for $d\gamma/dx$ as a function of doping; for example, $d\gamma/dx = 2.4$ mJ mol^{-1} K^{-2}/at.%(P) at $x = 0.25$. Integration of the smooth lines in Fig. 8(a) rescaled by this factor results in $\gamma(x)$ shown in Fig. 8(b). γ increases with doping in the underdoped region, has a sharp maximum at optimal doping, and then decreases with further doping. Also shown are measured values[38] of γ, which agree reasonably well considering the assumptions and uncertainties of our approach and the uncertainties in the values of γ. The overall behavior of $\gamma(x)$ is very similar to what has been observed in Co-doped Ba122, where the initial increase in γ was argued to result from the gradual suppression of the SDW order with Co doping.[9,29] Clearly, similar physics is at work in the P-doped system. On the other hand, a sharp increase of γ would also be expected from the presence of a quantum critical point close to optimal doping.

VII. CONCLUSIONS

We have studied the isovalently substituted system P-Ba122 by means of high-resolution thermal-expansion measurements. Using these data, we have determined the phase diagram via a thermodynamic probe, have studied the coupling of the SDW and superconducting order parameters, and have determined various pressure dependencies of the normal and superconducting states. Overall, we find surprisingly many similarities between the P-Ba122 thermal-expansion data and those of the supposedly electron-doped Co-Ba122 system. Not only the phase diagrams, but also the uniaxial pressure derivatives of the transition temperatures, as well as the coupling of the order parameters, turn out to be very similar in both systems. Both kinds of substitution can also be directly linked to uniaxial pressure, and both systems display a maximum of the Sommerfeld coefficient at optimal doping. This begs the question of why these systems behave so similar, in spite of the presumably different routes (chemical pressure versus electron doping) to superconductivity. Recent studies by Zinth *et al.*,[40] in which Ba122 was codoped with both Co and P, may actually throw some light on this question. These authors found that Co and P substitutions act in an additive fashion for suppressing SDW order and inducing superconductivity, whereas the opposite behavior was found for Co and K substitutions.[41] Further, it was argued that P content and physical pressure are also additive[7] and that the primary effect of both is to reduce the Fe-As(P) bond length.[40] In fact, Co-Ba122 also exhibits a very similar decrease of this bond length with Co doping,[8] which may explain why both kinds of substitutions act in a similar and additive manner. This may also explain the similarities of the uniaxial pressure effects determined in both systems using thermal-expansion data (this work and Ref. 9). Uniaxial pressure applied along the c axis, which most likely reduces the Fe-As distance and, as we have shown here, is proportional to P substitution, is predicted by the Ehrenfest relation to suppress the SDW order in both systems. This, we note, is in good agreement with recent theoretical predictions of the pure Ba122 system under uniaxial pressure.[35] Finally, we suggest that further detailed studies of the Fermi surface as a function of (uniaxial) pressure and doping are needed to better disentangle the distinct roles of doping and structural changes (i.e., chemical pressure) in determining the electronic properties of these interesting materials.

ACKNOWLEDGMENTS

We cordially thank J. Schmalian, T. Iye, and I. Eremin for discussions. This work was supported by the Deutsche Forschungsgemeinschaft through SPP 1458, by the Research Grants Council of Hong Kong, Grants No. 603010 and No. SEG_HKUST03, and by a Grant-in-Aid for the GCOE program "The Next Generation of Physics, Spun from Universality and Emergence" from MEXT, Japan.

[1]M. Rotter, M. Tegel, and D. Johrendt, Phys. Rev. Lett. **101**, 107006 (2008).
[2]A. S. Sefat, R. Jin, M. A. McGuire, B. C. Sales, D. J. Singh, and D. Mandrus, Phys. Rev. Lett. **101**, 117004 (2008).
[3]S. Sharma, A. Barathi, S. Chandra, V. R. Reddy, S. Paulraj, A. T. Satya, V. S. Sastry, A. Gupta, and C. S. Sundar, Phys. Rev. B **81**, 174512 (2010).
[4]S. Jiang, H. Xing, G. Xuan, C. Wang, Z. Ren, C. Feng, J. Dai, Z. Xu, and G. Cao, J. Phys.: Condens. Matter **21**, 382203 (2008).
[5]S. Kasahara, T. Shibauchi, K. Hashimoto, K. Ikada, S. Tonegawa, R. Okazaki, H. Shishido, H. Ikeda, H. Takeya, K. Hirata, T. Terashima, and Y. Matsuda, Phys. Rev. B **81**, 184519 (2010).
[6]P. L. Alireza, Y. T. C. Ko, J. Gillett, C. M. Petrone, J. M. Cole, G. G. Lonzarich, and S. E. Sebastian, J. Phys.: Condens. Matter **21**, 012208 (2009).
[7]L. E. Klintberg, S. K. Goh, S. Kasahara, Y. Nakai, K. Ishida, M. Sutherland, T. Shibauchi, Y. Matsuda, and T. Terashima, J. Phys. Soc. Jpn. **79**, 123706 (2010).
[8]S. Drotziger, P. Schweiss, K. Grube, T. Wolf, P. Adelmann, C. Meingast, and H. v. Löhneysen, J. Phys. Soc. Jpn. **79**, 124705 (2010).
[9]C. Meingast, F. Hardy, R. Heid, P. Adelmann, A. Böhmer, P. Burger, D. Ernst, R. Fromknecht, P. Schweiss, and T. Wolf, Phys. Rev. Lett. **108**, 177004 (2012).
[10]H. Shishido, A. F. Bangura, A. I. Coldea, S. Tonegawa, K. Hashimoto, S. Kasahara, P. M. C. Rourke, H. Ikeda, T. Terashima, R. Settai, Y. Ōnuki, D. Vignolles, C. Proust, B. Vignolle, A. McCollam, Y. Matsuda, T. Shibauchi, and A. Carrington, Phys. Rev. Lett. **104**, 057008 (2010).
[11]J. G. Analytis, J.-H. Chu, R. D. McDonald, S. C. Riggs, and I. R. Fisher, Phys. Rev. Lett. **105**, 207004 (2010).
[12]C. J. van der Beek, M. Konczykowski, S. Kasahara, T. Terashima, R. Okazaki, T. Shibauchi, and Y. Matsuda, Phys. Rev. Lett. **105**, 267002 (2010).
[13]Y. Nakai, T. Iye, S. Kitagawa, K. Ishida, H. Ikeda, S. Kasahara, H. Shishido, T. Shibauchi, Y. Matsuda, and T. Terashima, Phys. Rev. Lett. **105**, 107003 (2010).
[14]D. K. Pratt, W. Tian, A. Kreyssig, J. L. Zarestky, S. Nandi, N. Ni, S. L. Bud'ko, P. C. Canfield, A. I. Goldman, and R. J. McQueeney, Phys. Rev. Lett. **103**, 087001 (2009).
[15]A. D. Christianson, M. D. Lumsden, S. E. Nagler, G. J. McDougall, M. A. McGuire, A. S. Sefat, R. Jin, B. C. Sales, and D. Mandrus, Phys. Rev. Lett. **103**, 087002 (2009).
[16]S. Nandi, M. G. Kim, A. Kreyssig, R. M. Fernandes, D. K. Pratt, A. Thaler, N. Ni, S. L. Bud'ko, P. C. Canfield, J. Schmalian, R. J. McQueeney, and A. I. Goldman, Phys. Rev. Lett. **104**, 057006 (2010).
[17]R. M. Fernandes and J. Schmalian, Phys. Rev. B **82**, 014521 (2010).
[18]H. Luetkens, H.-H. Klauss, M. Kraken, F. J. Litterst, T. Dellmann, R. Klingeler, C. Hess, R. Khasanov, A. Amato, C. Baines, M. Kosmala, O. J. Schumann, M. Braden, J. Hamann-Borrero, N. Leps, A. Kondrat, G. Behr, J. Werner, and B. Büchner, Nat. Mater. **8**, 305 (2009).
[19]J. T. Park, D. S. Inosov, C. Niedermayer, G. L. Sun, D. Haug, N. B. Christensen, R. Dinnebier, A. V. Boris, A. J. Drew, L. Schulz, T. Shapoval, U. Wolff, V. Neu, X. Yang, C. T. Lin, B. Keimer, and V. Hinkov, Phys. Rev. Lett. **102**, 117006 (2009).
[20]D. S. Inosov, A. Leineweber, X. Yang, J. T. Park, N. B. Christensen, R. Dinnebier, G. L. Sun, C. Niedermayer, D. Haug, P. W. Stephens, J. Stahn, O. Khvostikova, C. T. Lin, O. K. Andersen, B. Keimer, and V. Hinkov, Phys. Rev. B **79**, 224503 (2009).
[21]E. Wiesenmayer, H. Luetkens, G. Pascua, R. Khasanov, A. Amato, H. Potts, B. Banusch, H.-H. Klauss, and D. Johrendt, Phys. Rev. Lett. **107**, 237001 (2011).
[22]F. Hardy, P. Adelmann, T. Wolf, H. v. Löhneysen, and C. Meingast, Phys. Rev. Lett. **102**, 187004 (2009).
[23]S. L. Bud'ko, N. Ni, S. Nandi, G. M. Schmiedeshoff, and P. C. Canfield, Phys. Rev. B **79**, 054525 (2009).
[24]A. E. Böhmer, P. Burger, F. Hardy, T. Wolf, P. Schweiss, R. Fromknecht, H. v. Löhneysen, C. Meingast, S. Kasahara, T. Terashima, T. Shibauchi, and Y. Matsuda, J. Phys. Conf. Ser. (to be published).
[25]C. Meingast, B. Blank, H. Bürkle, B. Obst, T. Wolf, H. Wühl, V. Selvamanickam, and K. Salama, Phys. Rev. B **41**, 11299 (1990).
[26]I. R. Fisher, L. Degiorgi, and Z. X. Shen, Rep. Prog. Phys **74**, 124506 (2011).
[27]E. van Heumen, R. Lortz, A. B. Kuzmenko, F. Carbone, D. van der Marel, X. Zhao, G. Yu, Y. Cho, N. Barisic, M. Greven, C. C. Homes, and S. V. Dordevic, Phys. Rev. B **75**, 054522 (2007).
[28]J. Hu, C. Setty, and S. Kivelson, Phys. Rev. B **85**, 100507(R) (2012).
[29]F. Hardy, P. Burger, T. Wolf, R. Fisher, P. Schweiss, P. Adelmann, R. Heid, R. Fromknecht, R. Eder, D. Ernst, H. v. Löhneysen, and C. Meingast, Europhys. Lett. **91**, 47008 (2010).
[30]E. C. Blomberg, A. Kreyssig, M. A. Tanatar, R. M. Fernandes, M. G. Kim, A. Thaler, J. Schmalian, S. L. Bud'ko, P. C. Canfield, A. I. Goldman, and R. Prozorov, Phys. Rev. B. **85**, 144509 (2012).
[31]C. Dhital, Z. Yamani, W. Tian, J. Zeretsky, A. S. Sefat, Z. Wang, R. J. Birgeneau, and S. D. Wilson, Phys. Rev. Lett. **108**, 087001 (2012).
[32]T. Iye, Y. Nakai, S. Kitagawa, K. Ishida, S. Kasahara, T. Shibauchi, Y. Matsuda, and T. Terashima, J. Phys. Soc. Jpn. **81**, 033701 (2012).
[33]A. Jesche, C. Krellner, M. de Souza, M. Lang, and C. Geibel, Phys. Rev. B **81**, 134525 (2010).
[34]We assume that the high-temperature value of α_c is doping independent, as seems to be the case for $\alpha_{\text{in-plane}}$. Variations of the measured high-temperature value of α_c are attributed to uncertainties arising from the tiny sample lengths along c ($\sim$70–150 μm). These deviations can be modeled with a correction factor between 0.9 and 1.3 to the lattice contribution for the different samples. The correction does not affect the shape of the anomalies.
[35]M. Tomić, R. Valentí, and H. O. Jeschke, Phys. Rev. B **85**, 094105 (2012).
[36]C. Chaparro, L. Fang, H. Claus, A. Rydh, G. W. Crabtree, V. Stanev, W. K. Kwok, and U. Welp, Phys. Rev. B **85**, 184525 (2012).
[37]S. K. Goh, Y. Nakai, K. Ishida, L. E. Klintberg, Y. Ihara, S. Kasahara, T. Shibauchi, Y. Matsuda, and T. Terashima, Phys. Rev. B **82**, 094502 (2010).
[38]Measured values of γ are taken from Fig. 2 for $x = 0.27$ and 0.33 and from Ref. 29 for $x = 0$. Values for $x = 0.30$, 0.33, 0.45, 0.5, and 0.55 are (also) obtained from the measured specific-heat jump $\Delta C/T_c$ (Ref. 36) using the empirical linear relationship $\Delta C/\gamma T_c = 0.066\ \text{K}^{-1} T_c$ valid for Co-Ba122 (Ref. 29).
[39]M. Matsunaga, Y. Ishikawa, and T. Nakajima, J. Phys. Soc. Jpn. **51**, 1153 (1982).
[40]V. Zinth and D. Johrendt, Europhys. Lett. **98**, 57010 (2012).
[41]V. Zinth, T. Dellmann, H.-H. Klauss, and D. Johrendt, Angew. Chem. Int. Ed. **50**, 7919 (2011).